Faculty of Sciences
Degree in Physics

Formation and Evolution of Galaxies in Cold Dark Matter Cosmology

Supervised by:
Dr. Chris Brook
Dr. Claudio Dalla Vecchia

Author:
Guacimara García Bethencourt

Academic year 2019/2020
San Cristóbal de La Laguna - July 2020

Acknowledgements

Este pequeño espacio está dedicado para todas esas personas que me han ayudado a lo largo del grado. Gracias especialmente a mi tutor Chris Brook por su ayuda y guía en el desarrollo de este trabajo, así como a Claudio Dalla Vecchia y al grupo de teoría del IAC. También me gustaría agradecer a mis compañeros de clase, profesores, amigos y amigas, a mis compañeras de piso, a mi familia. Gracias por todo.

Table of Contents

Abstract

El modelo cosmológico estándar actualmente aceptado es el ΛCDM, que establece una formación jerárquica de las galaxias a gran escala a partir de pequeñas fluctuaciones de densidad observadas en el Fondo Cósmico de Microondas. En este Trabajo de Fin de Grado se ha tomado una simulación numérica perteneciente al programa MAGICC y generada con el código `Gasoline`. Se ha utilizado el paquete de Pynbody, escrito en Python, para analizar esta simulación de una galaxia similar a la Vía Láctea y compuesta por unos 8 millones de partículas de estrellas, gas y materia oscura. Con el objetivo de obtener una distribución final de estrellas ex-situ (formadas fuera de la galaxia) en la galaxia a la edad actual del Universo, se ha analizado su formación a partir de las galaxias satélite que orbitan a su alrededor desde épocas tempranas. Primero, se han estudiado las abundancias de las estrellas, comparando las de aquellas que se forman in-situ (dentro de la galaxia) y aquellas que provienen del exterior, y distinguiendo la edad de mayor actividad de acreción ("merger epoch"). Se han identificado y rastreado varias galaxias satélite, observando su evolución con el tiempo hasta el momento en el que empiezan a formar parte de la galaxia central con dos métodos distintos. El primero, y el que finalmente se ha tomado para obtener los resultados, trata de tomar como referencia la estrella más antigua situada en el centro de cada satélite. El segundo método, se basa en una función específica de Pynbody que permite enlazar partículas entre dos capturas temporales ("snapshots") distintas de la misma simulación. Una vez obtenido el tiempo de acreción de varios "mergers" (galaxias satélite que se fusionan con la central), se han elegido 8 de ellos y se han anotado los valores de sus masas en el momento antes de su acreción. Luego, se han proyectado sus estrellas desde dicho instante hasta sus posiciones finales dentro de la galaxia. Así, se ha comprobado que, a priori, las estrellas de galaxias con menor masa y acretadas en edades más tempranas tienden a concentrarse en el centro de la galaxia principal en estructuras más o menos esféricas. Por otro lado, las galaxias más masivas y con tiempos de acreción mayores, son propensas a estar más dispersas y a extenderse más en la dirección radial. En definitiva, este trabajo ha permitido el estudio de la formación y evolución de una galaxia espiral desde edades tempranas dentro del marco cosmológico del modelo de concordancia del Big Bang. Asimismo, los resultados han permitido estudiar las distribuciones de estrellas externas, provenientes de estas galaxias satélite y compararlas según sus masas y tiempos de acreción.

Chapter 1

Introduction

Actualmente, la formación y evolución de galaxias a gran escala viene establecida por el Modelo ΛCDM. Este modelo se basa en las pequeñas fluctuaciones de densidad observadas en el Fondo Cósmico de Microondas, que produjeron una formación jerárquica de las diferentes estructuras a partir de densas zonas de materia oscura que comenzaron a atraer materia bariónica progresivamente gracias a la interacción gravitatoria. Estos y otros procesos pueden ser estudiados gracias a simulaciones numéricas como la empleada en este trabajo, donde el objetivo principal ha sido analizar una galaxia similar a la Vía Láctea y su formación a partir de galaxias satélite.

Currently, it is well established that the formation and evolution of galaxies at large scales is well predicted within the Cold Dark Matter (ΛCDM) paradigm. This is the modern standard cosmological model, based on Einstein's theory of General Relativity and on the *cosmological principle*, that states the Universe is homogeneous and isotropic on large scales.

The ΛCDM model bases the formation of galaxies on small initial density fluctuations observed in the Cosmic Microwave Background (CMB) (Penzias and Wilson, 1965), a remnant of the radiation left by the Big Bang when the Universe became transparent to electromagnetic radiation at the age of 380000 years, as temperature fluctuations by ESA's Planck satellite (P. Collaboration et al., 2013). These anisotropies found in the CMB are the result of dark matter decoupling from the rest of energy forms as the Universe expanded and cooled down after the inflation. The aforementioned instabilities caused a progressive assembly via gravity of more dark matter particles, leading to the development of potential wells that started accreting baryonic mass thanks to the gravitational interaction between dark matter

and baryons. These growing over densities of matter also began to merge into each other to form bigger systems. Thus, an hierarchical structure formation is presented through the creation of these dark matter halos in which each galaxy is embedded, carrying out the aggregation of gas and other particles, that allows the growth of the system and the formation of a disc via the conservation of angular momentum.

The collapse and merging of dark matter halos are the starting point and the trigger of galaxy formation. From this moment on, other phenomena such as star formation, stellar feedback (supernovae, stellar winds,...), Active Galactic Nuclei (AGN) and Super Massive Black Hole (SMBH) feedback, gas cooling, hydrodynamics, etc. begin to take part in order to run the entire galaxy evolution.

Figure 1.1: Milky Way's plane in an edge-on view perspective from Earth. Along with all the gas and dust and the bright zones filled with thousands of stars, some of the Milky Way's satellite galaxies can be observed. For instance, two dwarf galaxies known as the Small and Large Magellanic Clouds can be seen on the right side, below the galactic center. The Andromeda galaxy or M31, the largest galaxy in the Local Group, is also visible on the left side, below the disk. Source: https://www.eso.org/public/images/eso0932a/. Figure credit: ESO/S. Brunier

Later on, galaxies can also feel the gravitational pull of other galaxies and face the collapse with them leading to the development of a new bigger galaxy, disrupting the aforementioned physical processes and changing the whole structure of the original systems. Minor galaxies or satellite galaxies can also be influenced by the tidal forces and ram pressure due to the proximity of a bigger body and merge the latter, injecting new gas and stars to the host halo.

Many numerical simulations have been developed to study the dynamics and morphology of galaxy evolution. They use gravity, hydrodynamics and a wide variety of physical processes to predict the formation of said structures and their evolution through time since their early on stages. Therefore, simulations try to match observations to better understand the whole process of galaxy evolution in the Cold Dark Matter framework.

1.1 Objectives

The main goal of this project is to study the evolution of a Milky Way-like galaxy and its merging scenario through time. An initial distribution of said system within its viral radius will be taken to analyse the formation of the stellar disc and track the trajectories of its satellite galaxies from its beginnings, when the universe was $\sim 0.1\ Gyr$ of age, to the present day, $\sim 13.8\ Gyr$ after the Big Bang. Therefore, it will be possible to make a distinction between the stars that formed inside the main halo (in-situ) and the stars that started becoming part of it thanks to the accretion of minor halos (ex-situ).

The objectives that this work aims are presented as follows:

- Study the merger history of a Milky Way-like galaxy and its evolution from the early stages of its formation.
- Trace the evolution of the satellite galaxies over the years to their time of accretion into the main galaxy.
- Obtain the final distribution of ex-situ stars inside the main galaxy.
- Compare the final distributions of ex-situ stars from earlier mergers and later mergers.

Chapter 2

The Simulations

La simulación cosmológica utilizada en este trabajo forma parte del programa MAGICC y pertenece al conjunto de simulaciones de alta resolución de formación de galaxias de MUGS. Se trata de una simulación de N cuerpos que en la que se aplican la Hidrodinámica Suavizada de Partículas y numerosos procesos físicos tratados a pequeña escala, como el enfriamiento y la difusión de metales, la formación de estrellas, y el feedback estelar, que proporcionan un Medio Interestelar apto para la evolución galáctica. Este tipo de simulaciones están constituidas por partículas de estrellas, gas y materia oscura, sometidas muchos procesos y condiciones que desencadenan su evolución.

The cosmological hydrodynamical simulation being used in this project is part of the Making Galaxies in a Cosmological Context (MAGICC) program (G. Stinson et al., 2012) and belong to the set of high-resolution galaxy formation simulations from the McMaster Unbiased Galaxy Simulations (MUGS)[1] (G. Stinson et al., 2010). MUGS is a project consisting in 16 simulated elliptical and spiral galaxies of different properties and formation histories. These simulations are generated by `Gasoline`[2] (Wadsley, Stadel, and Quinn, 2004), a both N-body and Smooth Particle Hydrodynamic (SPH) (Monaghan, 1992) code designed for astrophysical problems that includes sub-grid physics such as, star formation, stellar feedback or radiative cooling, among others. Thus, `Gasoline` is able to efficiently resolve systems which gravity and hydrodynamics are the essential ingredients of their evolution.

On the other hand, for the analysis of the simulation at issue, it will be

[1] http://mugs.mcmaster.ca/description.html
[2] https://gasoline-code.com/

used the Pynbody[3] package (Pontzen et al., 2013), written in Python and based to analyse N-body and SPH simulations. Moreover, most of the analysis has been done thanks to the connection to the supercomputer *LaPalma*, located in the CALP (Centro de Astrofísica de La Palma), that constitutes one of the nodes that belong to the RES (Red Española de Supercomputación).

2.1 Cosmological Initial Conditions

The simulated galaxy analysed in this study is a late-type isolated galaxy with similar total mass than the Milky Way whose MUGS label is given as g15784. It has a total of ~ 8 million particles (stars, gas and dark matter) residing in a cube of $\sim 70\ Mpc$ on each one of its sides. The cosmological parameters of the simulation are the following ones: $H_0 = 73\ km\ s^{-1} Mpc^{-1}$ for the Hubble constant, $\Omega_\Lambda = 0.76$ for the density associated to the cosmological constant, Λ, and $\Omega_0 = 0.24$ for the mass density of the universe. These values agree with the Wilkinson Microwave Anisotropy Probe Three (WMAP3) (Spergel et al., 2006) observations of the CMB .

2.2 Sub-grid physics

`Gasoline` implements multiple sub-grid physics models, aimed to resolve small scale problems within the simulation that influence the evolution of the system on larger scales, that are resolved by the simulation. Here, the most important ones to consider are metal cooling and diffusion, star formation and stellar feedback.

2.2.1 Metal Cooling and Diffusion

The construction of an eligible environment to correctly evolve the simulation is realized via the application of sub-grid physics models such as metal cooling due to Hydrogen, Helium and several metal lines (Shen, Wadsley, and Stinson, 2009). This is done using the `CLOUDY` code (Ferland et al., 1998) and implementing an UV ionising background in equilibrium (Haardt and Madau, 1996) and Compton cooling, that provide photoionisation and heating to the Interstellar Medium (ISM). Metal diffusion is also taken into account and metals are then, dispersed through the gas through the usage of a turbulence model (Wadsley, Veeravalli, and Couchman, 2008).

[3] https://pynbody.github.io/pynbody/

2.2.2 Star Formation

Another important sub-grid physics model to consider is the star formation phenomena. These events take place when gas cools below a specific temperature ($T < 10000\ K$) and reaches the density of $n_{th} > 9.3\ cm^{-3}$, setting off the star formation processes. The threshold density expressed above is defined according to the characteristic width of the SPH kernel (Greg Stinson et al., 2006), through the imposition of a minimum smoothing length of 0.25 times the gravitational softening length, which has the value of $\epsilon = 155\ pc$. The setting up of this limit and the adding of a pressure field in star formation areas with high density (Robertson and Kravtsov, 2007) of gas, avoid the collapse of gas particles to distances beyond the SPH spatial resolution. The amount of gas that is turned into stars is given by the Kennicutt-Schmidt law (Schmidt, 1959; Kennicutt, 1998):

$$\frac{\Delta M_\star}{\Delta t} = c_\star \frac{M_{gas}}{t_{dyn}} \tag{2.2.1}$$

where $\Delta M_\star$ is the mass of the star particles formed, Δt the timestep between star formation events, $c_\star$ is the star formation efficiency, M_{gas} the mass of the gas particles, and t_{dyn} their dynamical time, i.e. the time gas requires to collapse to form a star. In this period, a fraction of gas will become star particles according to the value of $c_\star = 0.167$ and depending on the stellar feedback.

The resultant star particles are collisionless and represent a cluster of stars with a Simple Stellar Population (SSP), using the Chabrier (Chabrier, 2003) Initial Mass Function (IMF) to represent its initial mass distribution.

2.2.3 Stellar Feedback

The energetic feedback injected by stellar processes helps to regulate star formation and metals distribution in the ISM. There are two types of stellar feedback implemented in this simulation: Early Stellar Feedback (ESF) (G. Stinson et al., 2012) and Supernovae (SN) feedback.

The ESF or pre-SN feedback consists in stellar energy from massive young stars in the form of thermal radiation, that inputs the 10% of the energy to the surrounding gas via stellar winds and photoionisation of the ISM. The second type of feedback is due to type Ia supernovae (SNIa) and type II supernovae (SNII) bursts, that introduce new energy and metals to the en-

vironment of the exploding star. SN feedback serves to rearrange the matter inside stars, returning it to the ISM, and to stop stellar formation in the surroundings by spreading and heating the gas. This process is implemented using the blast-wave formalism (Greg Stinson et al., 2006), that prevents the resulting energy from the explosion to be radiated away on unphysically short timescales due to the code's resolution limits. Accordingly, cooling needs to be turned off within the blast-wave radius in order to ensure effective feedback on the scales that the simulation resolves.

2.3 Simulated Galaxy characteristics

The zoom simulation studied in this project has a value of $\sim 38444\ M_{\odot}$ for the mean stellar particle mass. It has ~ 4 million particles within its virial radius at redshift $z = 0$. The total, stellar and gas masses within the virial radius are shown in table 2.1:

	$M\ [M_{\odot}]$	$M_{star}\ [M_{\odot}]$	$M_{gas}\ [M_{\odot}]$	$R_{vir}\ [kpc]$
g15784	150.70×10^{10}	8.28×10^{10}	1.35×10^{11}	325.68

Table 2.1: Simulation data

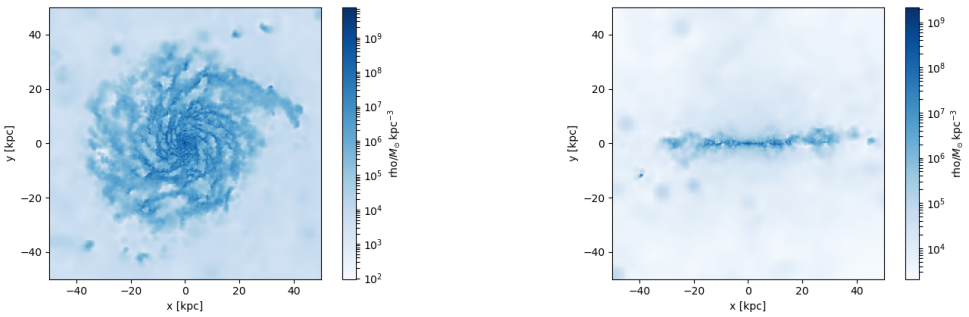

Figure 2.1: Density map of the gas in the simulated galaxy. In this picture, two panels of 50x50 kpc show the density of gas in a face on view and a side on view. The dark blue colours represent regions with high density of gas, while the white coloured zones have a low density of gas particles.

Chapter 3

Methodology

El procedimiento aplicado para analizar la formación de la galaxia simulada a partir de sus galaxias satélite y su evolución con el tiempo se ha basado en el concepto de Arqueología Galáctica. Inicialmente, se han estudiado las abundancias de las estrellas presentes en la simulación y luego, se han identificado las galaxias satélite en edades tempranas para rastrearlas hasta el momento de su acreción por dos métodos distintos: el primero, basado en tomar una estrella antigua del centro de cada galaxia como referencia; y el segundo, aplicado gracias a una función específica de Pynbody que conecta las partículas entre dos momentos diferentes de la simulación. Por último, se toman las estrellas de cada galaxia justo antes de empezar a formar parte del halo principal para estudiar su distribución final.

To achieve the main goal of this project of identifying the stellar populations that formed ex-situ (outside of the Milky Way-like galaxy), I have taken the stars of some satellite galaxies that formed at early times in the outskirts of the main halo (that hosts the main galaxy in the simulation). These satellites, located within virial radius of the main halo, are traced through several snapshots of the simulation to study their evolution with time (their trajectories around the proto-galaxy and their merging with other minor halos) until they get accreted by the main halo and start being part of it. Eventually, I have searched for the positions of those merged stars inside the main halo at redshift zero, i.e. at the current age of the Universe, obtaining the stars that did not formed inside the stellar halo or the stellar disc of the galaxy.

This process is similar to the observational research based on *Galactic Archaeology*. While here, we try to tell the current state of the stars by tracking them from their origin in nuclear clouds outside the main halo thanks to nu-

merical simulations. *Galactic Archaeology* studies the formation and merging history of galaxies via the analysis of stellar properties observed in the present day, thank to data provided by missions like *Gaia* (G. Collaboration et al., 2018) and many spectroscopic surveys such as APOGEE (Majewski et al., 2017). Thus, properties such as metallicity allow us to know the chemical composition of the interstellar medium where the stars got their gas and elements. According to this type of investigations, we now know that stars with similar chemical abundances come from a common progenitor. On the other hand, the study of kinematical properties (velocities, orbital eccentricity, etc.) gives us information such as the trajectories that the stars follow inside the galaxies, pointing out the movement they had before being accreted since they tend to maintain similar paths. This can also tell us the angle of accretion of a certain merger, giving a clue on how its orbit around the galaxy was in the past and therefore, where its stars come from. Besides, other important property such as the age of the stars can be used to create a timeline of the events that led to the formation of the different components of the galaxy. Hence, all of these properties permit us to know the origin of the stars located in the stellar halo or in the stellar disc of certain galaxy, reconstructing their history and evolution, whether they got accreted from an outer minor halo or not.

3.1 Chemical abundances

As mentioned before, the metallicity or abundance of the stars gives us information about the chemical composition of the molecular cloud where they come from (this type of research is known as chemical "tagging" (Freeman and Bland-Hawthorn, 2002)). This means that stars with different metallicities will have different origins, so if we analyse the evolution of the abundances of the stars in the main halo through time, we will be able to have a general view of the merger history of the simulated galaxy. This can be done by plotting the [Fe/H] content with respect to time to obtain a density map of the stars that have lower or higher abundances (with respect to the Sun). The value of the iron-to-hydrogen ratio of the stars indicates the iron abundance compared to the Sun that each stellar population have at a certain moment of their life in the simulation. The same way, the magnitude [O/Fe] represents the oxygen-to-iron ratio with respect to the Sun, and [O/H] shows the oxygen-to-hydrogen ratio, all calculated in a logarithmic scale and measured in units of "dex" (decimal exponent).

As we can see in figure 3.1, the vertical axis represents the abundances and

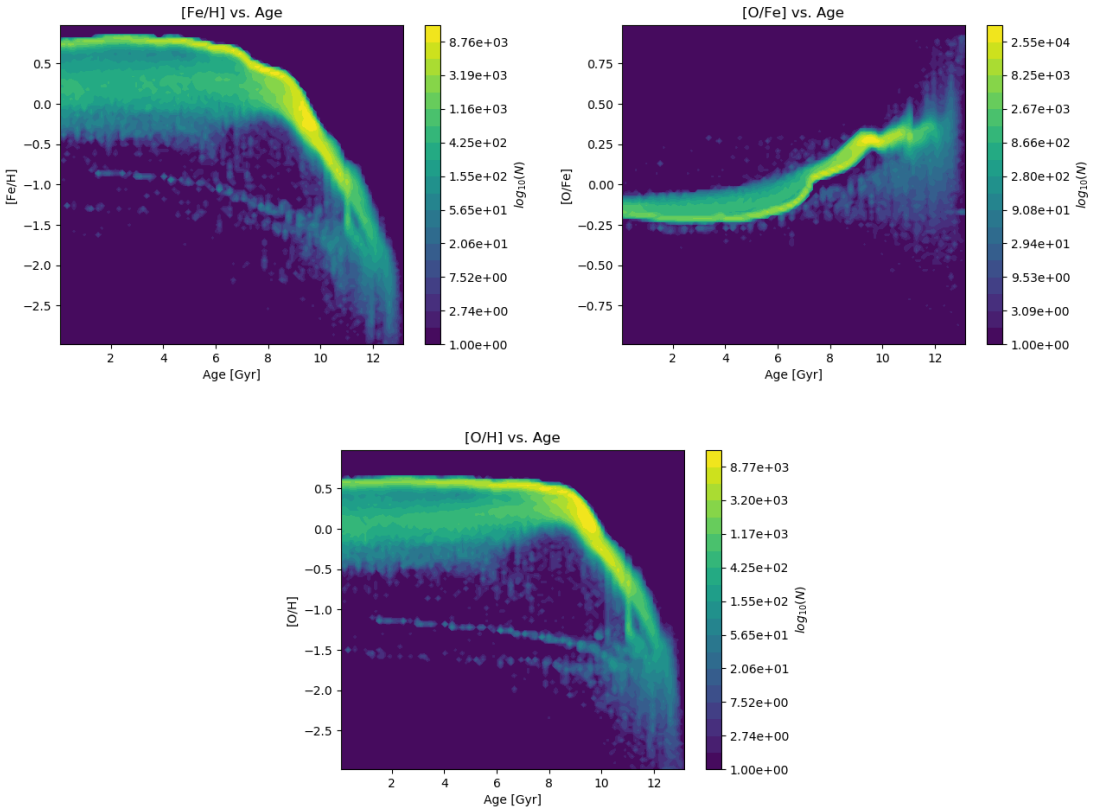

Figure 3.1: Metallicities of the present stars in the system with respect to their ages. The left top panel shows the iron-to-hydrogen content through the years, while the right top panel and the bottom panel show the oxygen-to-iron content and the oxygen-to-hydrogen content, respectively.

the horizontal axis the age of the stars present at the current time. Therefore, the oldest stars, born in the early stages of the formation of the galaxy, are represented on the right side of the plot, while the youngest stars, that were formed much later, are shown on the left. On the other hand, the colour of the map shows the number of stars with a certain metallicity at a certain age. Thus, the yellow regions of the map correspond to larger amounts of stars, while the purple ones correspond to a shorter number of stars. The well-defined yellow trends that these plots show, where most of the stars are located, represent the abundance evolution of the stars formed in the main halo, i.e. the stars that formed in-situ. Besides, the bright trails with the highest values of the abundances in the [Fe/H] and [O/H] plots (and the lowest in the [O/Fe] plot) correspond to stars that formed in the most metal-rich parts of the galaxy, i.e. the inner regions of the disc and the bulge. The

large scattering below these trails (and above in the [O/Fe] plot) for young stars are due to stars born in the outer regions of the galaxy, which are more metal-poor and have a less polluted gaseous environment.

In the [Fe/H] and [O/H] plots, it is easy to see how the abundances of the stellar populations increase as time goes by in the simulation (from right to left), i.e. younger stars (0-9 Gyr of age) have higher abundances than older stars (9-13 Gyr of age), that present a wide range of values of the iron-to-hydrogen and oxygen-to-hydrogen contents. This rising trend is due to the progressive pollution of the ISM by supernovae (Type Ia and II), that introduce new metals to the environment with time, making the gas in the galaxy to be more metal-rich when forming new stars. On the other hand, from the [O/Fe] plot, we can say that younger stars have lower oxygen-to-iron content than older stars. This happens because Fe is mainly produced at later times (in SNIa explosions) than Oxygen (which is formed rapidly in SNII), so that the amount of iron increases with respect to that of the oxygen with time, causing the oxygen-to-iron ratio to decay for stars that form later.

In the framework of the ΛCDM model, the structure formation of a disc galaxy like the one we study here is given by an hierarchical merging of minor halos and satellite galaxies that orbit around a bigger potential well with higher density, that corresponds to the main halo or the proto-galaxy. These mergers were more frequent at early times, due to the higher density of the Universe in the past. This greater number of mergers can be observed by the scattering of abundances at early times, mainly in the [Fe/H] and [O/H] plots in figure 3.1. Here, a wide range of metallicities can be seen at the beginning of the formation of the galaxy, corresponding the lower values of iron-to-hydrogen and oxygen-to-hydrogen ratios to the stars from minor satellites that got accreted into the main halo. This period of time with high accretion activity is called the "merger epoch". The faint colour of all of these stars shows us that the mergers were not as dense in stellar particles as the main halo, because they were much smaller. It is also possible to note two minor second trends in the plots, corresponding to stars with lower abundances and a large range of ages. These stars are part of an ongoing merger event at later times in the merger history of our simulated galaxy. We can say from this fact that this galaxy is the result of the collapse of two original galaxies, a bigger and denser one (the main halo) and a smaller body that got disrupted due to the tidal forces and eventually, accreted into the larger structure. An even fainter third trend is visible in these plots, probably due to other merger event at the same epoch but much smaller than the others. In the [O/Fe] plot, where the values tend to decrease with

time, these paths are not so clear, but it is discernible the main one and the dispersion caused in the "merger epoch", due to the stars stemming from smaller halos.

Thus, all of these old stars that have lower metallicities in the [Fe/H] and [O/H] maps, come from outside of the main halo via mergers during the formation and evolution of the galaxy. In this report, I am going to explain how I traced some of these mergers and their stars all the way to their final position in the stellar structure of the major galaxy.

3.2 Analysis of the merger history of the galaxy

As mentioned in previous sections, the zoom simulation studied in this project is a Milky Way-like isolated galaxy with a high merger activity in the early Universe and less merger events at later times, although we will see an ongoing merger at the end of the simulation. Both its stellar disc and its stellar halo can be seen from the pictures in figure 3.2 as a density stellar map in a faced on orientation and a sided on orientation. In the picture, we can observe the main galaxy at the centre and some other minor galaxies and structures in the surroundings, that are being dragged by the gravitational pull of the bigger body. It is also clear to see one of these satellite galaxies as a long stream of stars because it is getting torn apart by the tidal forces and its stars are starting to become part of the main halo. This satellite is currently being accreted by the main galaxy. In this project, I focused in the "merger epoch" that took place long time before this big merger event, from around redshift z = 4.7 (Universe of $\sim$ 1.30 Gyr of age) to redshift z = 1.5 (Universe of $\sim$ 4.00 Gyr), but I also traced minor mergers at later times down z = 0.60 (Universe of $\sim$ 8.00 Gyr).

In figure 3.2 there are two 325x325kpc panels shown, according to the virial radius of the main halo at current time. This value is defined using all mass inside a given density and here, it has been calculated as the maximum radial position of all the dark matter particles in the main halo. Therefore, we create an spheroidal limit around the centre of the dark halo with a radius of 325 kpc.

3.2.1 Identifying the halos

The first step to analyse the satellite galaxies in this simulation is to determine their halo number. This number is an identifier of each halo for

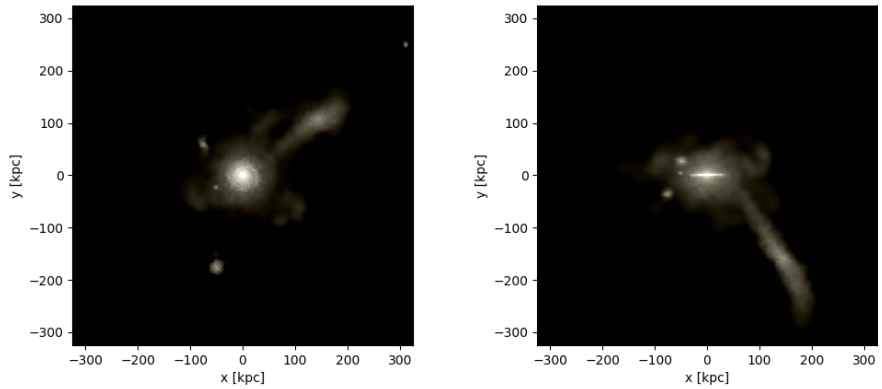

Figure 3.2: Stellar distribution of the simulated galaxy at the current age of the Universe (redshift z = 0.02) shown in a faced on orientation (left) and in a sided on orientation (right). This snapshot contains all the particles within a range from -325 to 325 in both the vertical and horizontal axis, according to the virial radius of 325 kiloparsecs. The stars are represented using the bands I, V and U.

every snapshot[1] so that they are sorted by number of particles. Thus, the larger halo is the main galaxy and it is labelled has halo one or h1. For this study, I have only taken into account halos that contain more than 20 stellar particles (disregarding small satellites) and with more than 50 dark matter particles, to make sure they have enough dark matter to be a galaxy and they are not just a star cluster.

The process I followed to identify the number of all the halos located within the virial radius was to search for all the halos whose centre position in cartesian coordinates was smaller than 325 kpc for both the x-axis and the y-axis. I classified these as "visible halos" and then, covered with coloured dots all the stellar particles in each satellite to visualize them like in figure 3.3[2].

The identifier number of these halos is not the same one in every snapshot due to the increase in the number of particles in the satellites when they merge another halo or the losing of particles caused by phenomena like collision, ram pressure or tidal stripping. For this reason, it is necessary a process to be able to identify the same satellites in different time steps. The method used here to carry out this tracking is based on choosing an old star

[1] In the simulation, a snapshot is a certain distribution of the system at a moment of time.

[2] This is done by plotting every dot in the position of the corresponding star according to their cartesian coordinates (x-axis and y-axis) in the snapshot at issue.

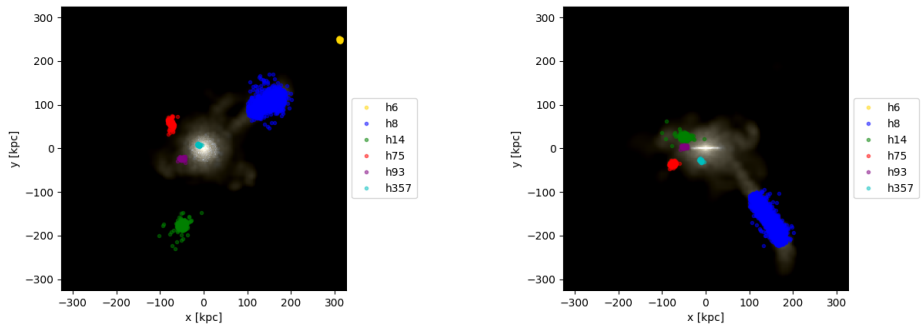

Figure 3.3: Satellite galaxies at the redshift z = 0.02. There are six satellite galaxies with more than 20 stars and more than 50 dark matter particles at the current time within the virial radius. Two of them can be seen very close to the centre of the main halo, about to merge. Halo h8, is the one that is being accreted as we can see by the stream of blue stars that is getting pulled by the bigger galaxy.

at the centre of the galaxies and it is explained in depth in the next section.

3.2.2 Tracing halos through time ("Old-Star method")

In order to track the evolution of the mergers and their stars over the years, an old star is taken from the centre of each halo and traced through every snapshot or time step until it becomes part of the main halo. In this way, that old star assures us that it has been inside the satellite galaxy at issue for a long time, so that we can assign it to its host halo as a fixed reference and trace all of its stars through the different time steps.

To carry out this method, I did an example first for the last snapshot i.e. at current time. By taking all the stars of each halo within a radius of 0.5 kiloparsecs from the centre and then, choosing the oldest one of them, I could record its identification number in the whole simulation, called "iord" number. The process of searching these stars is done in a similar way than for the aforementioned process of pinning down the satellite galaxies inside the virial radius of the main halo. Thus, I looked for the centre of the satellite at issue and save all the "iord" values of those stars whose radial position was smaller than 0.5 kpc. At this redshift (z = 0.02 at the current time), these stars are very old, ranging from 10 to 13 gigayears of age.

With the identification number of these old stars saved, I loaded the two previous snapshots (at redshift z = 0.03 and z = 0.05), which corresponded to an age of the Universe of 13.30 and 13.09 Gyr, respectively. To know the

position of these fiducial stars at said moments of time, I looked for their "iord" number in every halo within the snapshots, except for the main halo (halo one or h1). Then, when the algorithm finds the star at issue in one of the satellites, its halo number is recorded and all its stars are covered in dots with the same colour as the original halo, taken at redshift z = 0.02.

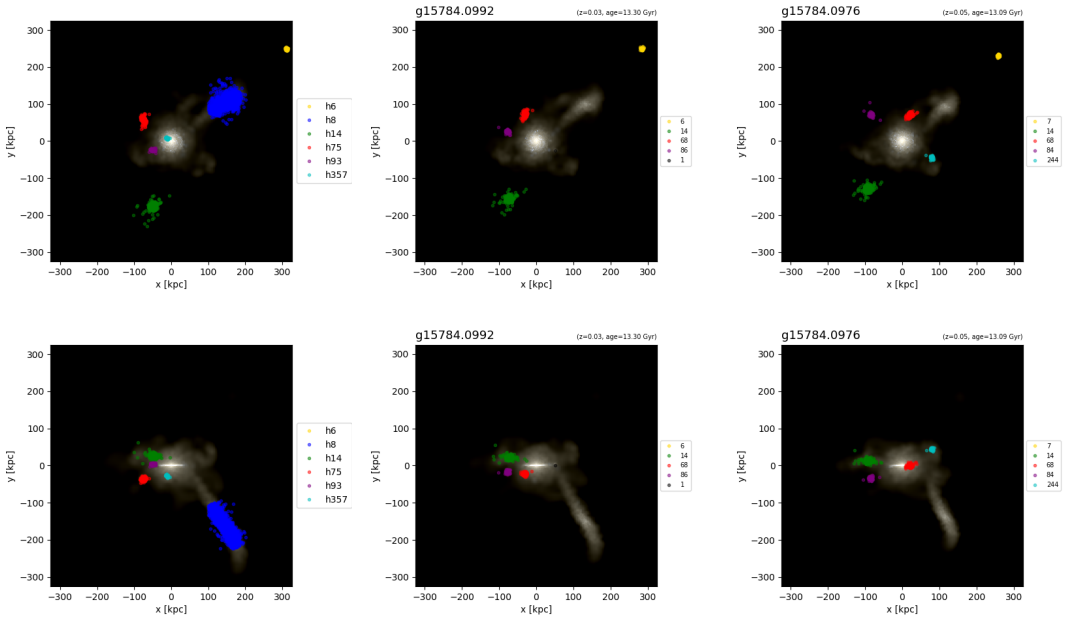

Figure 3.4: The halos found within the virial radius at the current time are traced from low redshift (z = 0.02) to higher redshift (z = 0.05) (from left to right), i.e. back in time, and tagged with colours according to the original satellite as follows: halo 6 in amber, halo 8 in blue, halo 14 in green, halo 75 in red, halo 93 in purple, halo 358 in cyan.

As it can be seen in figure 3.4, halos h6, h14, h75 and h93 are pointed out in amber colour, green, red and purple, respectively. Their corresponding halo number in the previous snapshots are h6, h14, h68 and h86 at redshift z = 0.03, and h7, h14, h68 and h84 at redshift z = 0.05. In particular, the number of halo h93 changes rapidly through the different snapshots in the way that it gets smaller to higher redshift. This means that the halo becomes larger in terms of number of particles when traced back in time, so it might have lost mass while orbiting around the main halo, due to tidal forces. On the other hand, halo h8, that is being accreted by the main galaxy and is marked in blue at current time, couldn't be traced because there was a problem in the algorithm that couldn't precise its centre, probably due to

its elongated structure. Since this halo is being disrupted and its stars might have changed their position during the time of infall, it might be difficult to trace it through the years since the chosen star could move from place to place inside the galaxy or even got ejected from it. On the other hand, halo h358 (coloured in cyan) does not appear as a satellite in the second snapshot but inside the main halo (the reference star is marked in black), and reappears as an independent minor halo in the third panel. This is due to a limitation in the code that defines the halos in Pynbody, called `AMIGA Halo Finder` or `AHF` (Gill, Knebe, and Gibson, 2004; Knollmann and Knebe, 2009), which characterises sub-halos according to high density regions of particles within the main halo. However, this definition might not be effective when a certain halo is being accreted because it loses mass and becomes less dense. Thus, in the snapshot shown in centre panel of figure 3.4 (correspondent to a redhsift of z = 0.03), the `AHF` halo finder might not been able to distinguish halo h358 as an independent halo and hence, assigns its stars to the main galaxy (halo 1). This difficulty in identifying sub-halos can also occur when the satellite is near to the galactic centre as the overall density is greater and the `AHF` code cannot make a contrast between the density of both halos.

Tracking the evolution of satellite galaxies from early stages

Once I tested the method in the example explained above, I started tracing the halos from higher redshift to lower redshift, following the same direction as the "arrow of time" in the simulation. Then, as for the example, I looked for the satellite galaxies with more than 20 stellar particles and more than 50 dark matter particles within the virial radius of 325 kpc (virial radius at redshift z = 0.02) at a redshift of z = 5.53, which corresponds to a Universe of 1.09 Gyr of age. In the figure 3.5, we can see the stars from 22 halos marked in several colours. This plot corresponds to one of the moments in the "merger epoch" of the simulated galaxy, in which it is still forming and accreting great amounts of matter that will generate the galactic disc.

The next step, was applying the "old-star method" described before to all of these halos so that I could take one fiducial star from each one and use its "iord" number to trace the whole satellite. When doing this, there was one halo (specifically, halo h17) that the algorithm missed because it did not have any star at its centre within a radius of 0.5 kpc. Hence, I increased this limit to the value of 2.0 kpc for all the satellites galaxies. Next, all the satellites shown in figure 3.5 were traced through several following snapshots.

In figure 3.6 we can see the evolution of the halos in three different time steps after redshift z = 5.53. In this timeline of snapshots, we can appreci-

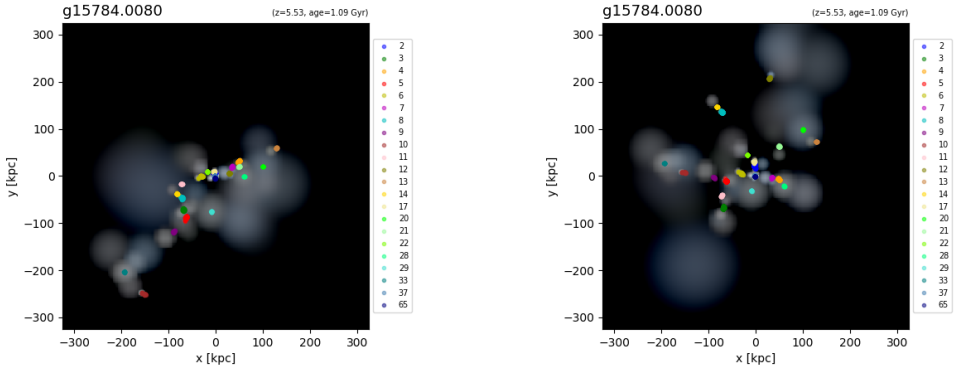

Figure 3.5: Satellite galaxies within a virial radius of 325 kiloparsecs at redshift z = 5.53. Twenty two minor halos, marked in different colours, are shown in a face on view (on the left) and a side on view (on the right).

ate the hierarchical formation of the simulated galaxy and how the satellite galaxies are joining together because of the gravitational pull of each other, as well as merging into the main halo while growing and becoming part of bigger structures with time. Some halos may not be seen because the colours from other halos could be plotted on top of them, but they are indicated in the legend. On the other hand, if an old star that is being traced for a certain halo starts to become part of the galaxy at the centre, it is considered that the whole satellite has merged. Then, it is marked with the number one, but keeping the colour of its original satellite so that we can know where it comes from. This condition is taken at the moment of searching for the corresponding host halos of each star in the subsequent snapshots, by looking for those stars in every single halo but the main one. Thus, if one of the old stars that are being traced does not appear in any of the satellites, it must be in the halo h1, the main galaxy. In the same way, these stars can reappear from halo h1 into some new satellite during its orbit around the centre, so they are tagged as a satellite again (in the third panels, halo h22 has reappeared from the main halo after being accreted between redshift z = 5.53 and redshift z = 4.79). Note also, that there are some stars that seem to be part of two satellites at once so their different halo numbers are shown with the same colour in the legend. These must be halos that are too close to each other or even overlapped (probably due to the limitations of the `AHF` halo finder) and share some stars. Lastly, there are also halos that have different colours for the same number, for instance, halo h11 in the last panels. This means, that two or more of the traced old stars have started becoming part of the same halo, i.e. their progenitors have merged together into a single structure.

One important issue to have in mind when applying the "old-star method" regards to the case when the reference star chosen infalls earlier than the rest of its host halo. In this case, if the old star starts to become part of the main galaxy before its satellite galaxy, the method considers that the whole halo has merged when it is actually still getting accreted. For this reason, it was found that a possible solution to this problem was constraining the velocity of the fiducial old star to low values. Therefore, the star would need to be close to the centre of the satellite galaxy and also have a low velocity with respect to its companions, so that it is well gravitationally bound to the centre and does not change much its position. However, there was not time during the development of the project to verify this matter.

Other interesting thing to observe in figure 3.6 is some filimentary structure in infalling satellites, indicating that they may be infalling from certain directions preferentially. They are also visible some hints of group infall (i.e. satellites that form groups during their accretion), e.g. halos 2, 4, 16, 17 and 30 in the central panels (snapshot 0112) seem to be grouped in a relatively small volume. However, there was not time in the project to further explore this.

Finding new satellite galaxies in subsequent snapshots

As time goes by in the simulation and minor halos merge together and become larger, they can appear new satellites above the limit of 20 stars and 50 dark matter particles in each one. In previous snapshots, these halos have been outside of this limit and have not been considered, but they must be taken into account when they get big enough. This is also applied for possible satellites that might come from the outskirts of the virial radius. Thus, as the system evolves and the satellites are tracked all the way to their infall moment, I have also looked for these new halos in each snapshot, taken an old star placed at their centres, and traced them through time along with the previous ones thanks to the "iord" number of these stars. Comparing the plots in figure 3.7 with the plots in figure 3.6, we can see some new halos that have arisen in each time step and then, are traced to the next one. Besides, most of these halos appear near the galactic centre or other group of halos due to the high density of matter in those regions, that causes the particles to gather up. The emergence of these new halos starts to decay at later stages in the formation of the galaxy, as they merge.

The process to find these new halos was to search for all the "visible halos" in each following snapshot within the radius of 325 kpc (as it was done for the first snapshot at redshift z = 5.53) and then, compare them to the ones that

have already been traced from higher redshift. Thus, only the satellites that have appeared in the snapshot at issue are tagged as new ones. Next, an old star is chosen from the centre of every new halo and its "iord" value is also compared with the ones from the previous halos to make sure there is not any repetition due to halos that might overlap. The radius within which the fiducial star is taken needed to be increased in some occasions for the reason that it might not be any star within the previous radius chosen. Depending on the satellites, different values were used such as 3.0 kpc or 4.0 kpc, but the default value was a radius of 2.0 kpc from the centre of the galaxy.

3.2.3 Bridge method

The Pynbody package has an algorithm implemented to trace particles between snapshots of the same simulation, called *Bridge module* [3]. This module is based on linking two snapshots together via an object called bridge, that connects a certain subset of particles from one time step to another. Therefore, using this module one can trace all the stellar particles belonging to each halo through time in the way that those original groups of particles are traced independently in every moment, without taking into account the fact that they merge others and become larger. However, the *Bridge module* also allow us to identify halos between snapshots via a function that matches their halo catalogues, so we can know when they merge or get accreted into the main halo. I have used these options provided by the *Bridge module* to compare them to the results from the "old-star method" explained in section 3.2.2.

Again, I made an example to visualize the results of this method with the satellite galaxies given at redshift z = 0.02. We can see in figure 3.8, by just linking the snapshots and tracing each one of the groups of stellar particles from one step to the previous one (panels above), all of them are correctly traced and pinned down. However, doing this the algorithm is not able to tell which halo they belong to. On the other hand, the panels below were done by linking the particles between snapshots and matching their halo catalogues, so the whole satellite is traced. Here, the algorithm misses some satellite galaxies but, unlike in the "old-star method", it is able to trace the halo that is being accreted by the main galaxy (blue halo)[4].

[3] https://pynbody.github.io/pynbody/tutorials/bridge.html

[4] There is a misprint in legend of the panels placed on the left, where halo h357 should be halo h358.

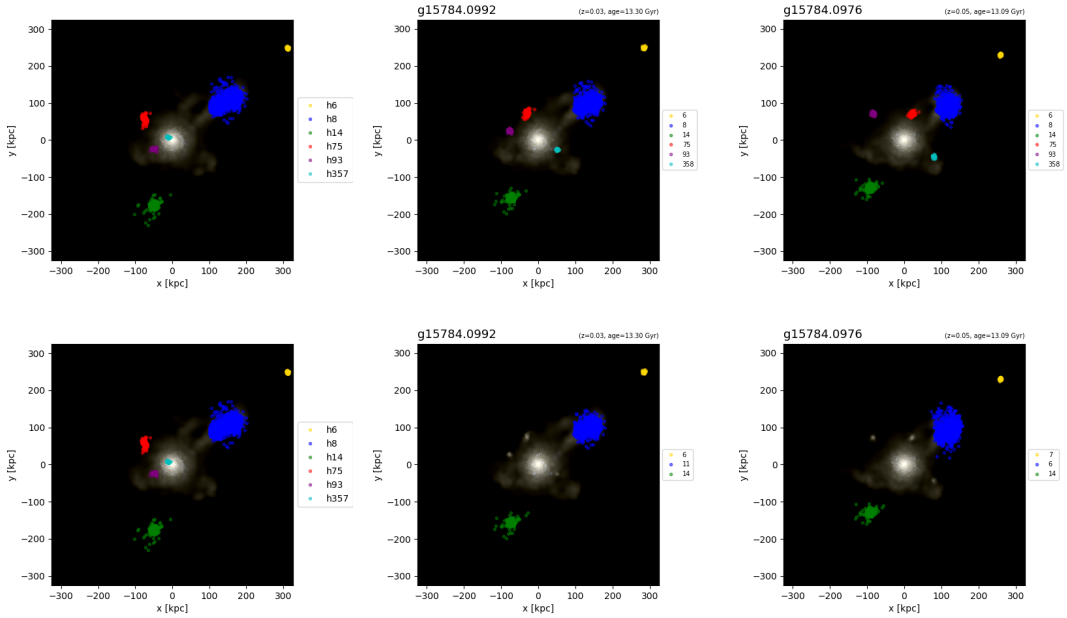

Figure 3.8: Halos traced from low redshift (z = 0.02) to high redshift (z = 0.05) (from left to right) using the Bridge method. The panels above show the results by just tracing all the stellar particles from the original satellites and the panels below show the results by using the halo match option from the *Bridge module* (in the panels below the halo number shown in the legend is the correspondent to the current snapshot, while in the panels above the halo number refers to the original satellite).

The results using this module with all the halos found in the first snapshot, at redshift z = 5.53 (not including the new halos found in posterior steps), are shown in figure 3.9. From the comparison with figure 3.6, we can see that there is no repetition in the colour of the satellites displayed in the legend. This is because this tracing method is not following one single star that may share two different halos that are overlapped or close to each other, but it is tracing the entire halo. Due to this doubling, the old star that seems to be in halo h2 and halo h19 in the last panel of figure 3.6 makes both halos to be coloured in pink. While, with the bridge method these two satellites are treated independently and coloured in red and pink, respectively. On the other hand, we can also observe how this method misses some satellites with respect to the "old-star method", i.e. it does not trace some of the halos. The *Bridge module* also shows some inconsistency regarding to the accretion time of each merger since there are halos that seem to merge before than in the "old-star method" and that are pointed out with number one. This is

because the bridge method traces the halos according to the position of the majority of their stars in each time step. Then, if more than a half of the total number of stellar particles of a certain satellite are in the main halo, the method considers it as accreted, i.e. belonging to the central galaxy. The main halo is coloured according to the colour of the last merger that is plotted in the picture (in the legend, the last satellite belonging to halo h1).

In the end, due to the missing satellites and the discrepancy between the infalling times of some of the halos this method was dismissed, and the analysis of the mergers was done with the "old-star method".

3.2.4 Mergers at the current age of the Universe

Once I traced all the satellites from several snapshots until the moment they merge the simulated galaxy (i.e. their old star of reference starts to become part of the main halo), I chose some of them for the study. The next step was tracing all the stellar particles in those mergers to the last snapshot, at redshift z = 0.02, so one could see their final position and distribution.

Then, to trace these mergers to the current age of the Universe, I saved the "iord" numbers of all the stars inside each halo in the snapshot before they merge the main galaxy. Next, looking for these identification numbers in the whole snapshot at redshift zero I could pin down their positions in the simulation at that time and therefore, cover every star from each progenitor with coloured dots to identify them inside the main halo. These results are presented in chapter 4 in more detail.

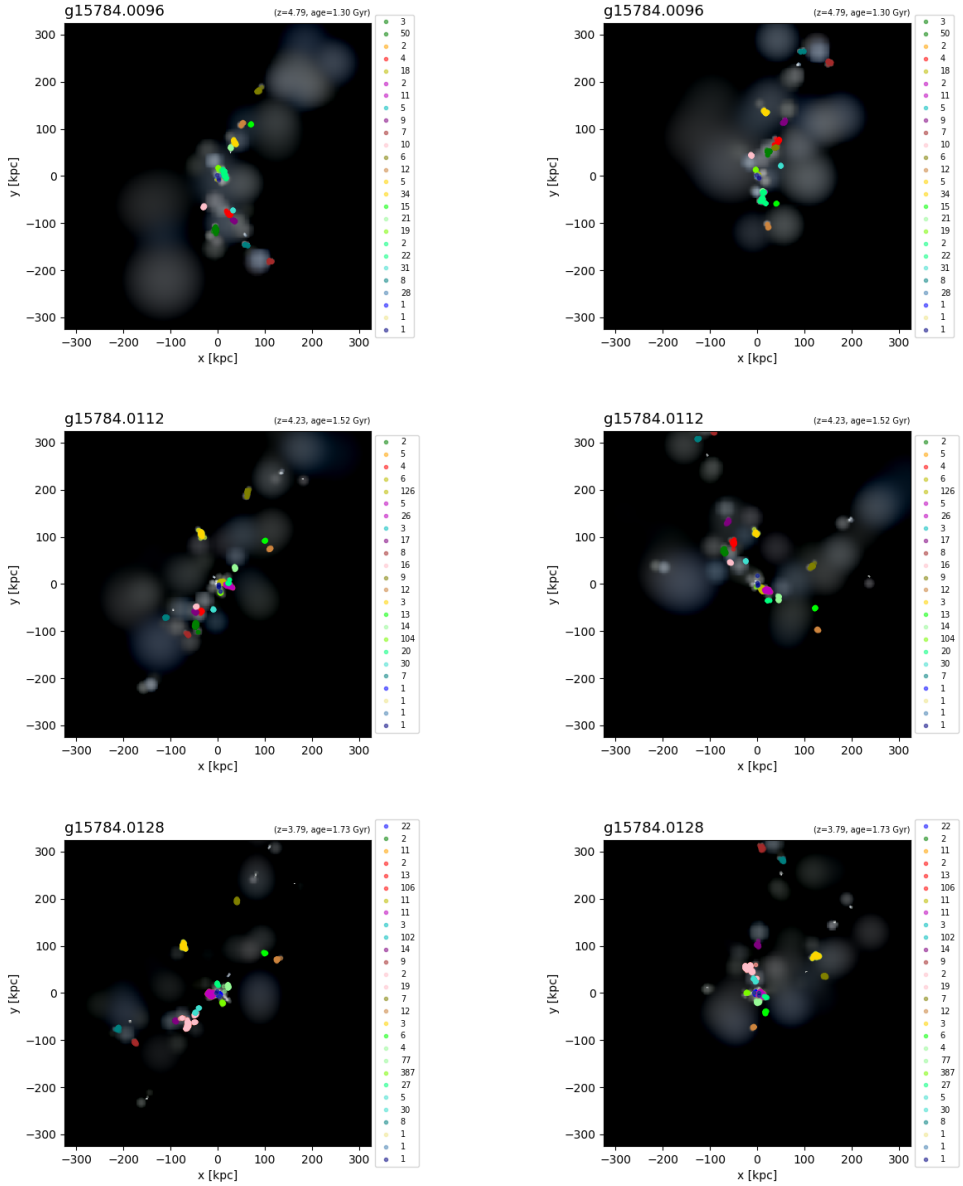

Figure 3.6: Satellite galaxies traced from higher redshift (above) to lower redshift (below). The redshifts range from z = 4.79 to z = 3.79. The first column (left) corresponds to a faced on perpective of the system and the second one (right) corresponds to an edge on perspective. All halos are shown with their current identification number in the snapshot at issue, instead of their original number. The colour of each halo is the same than the original halo at high redshift thus, they can be distiguised by their colour. The old stars that start to become part of the main halo in each time step and therefore, it is considered that their progenitor satellite has merged the bigger galaxy (halo h1), are denoted by number one but keeping the same colour of their original halo.

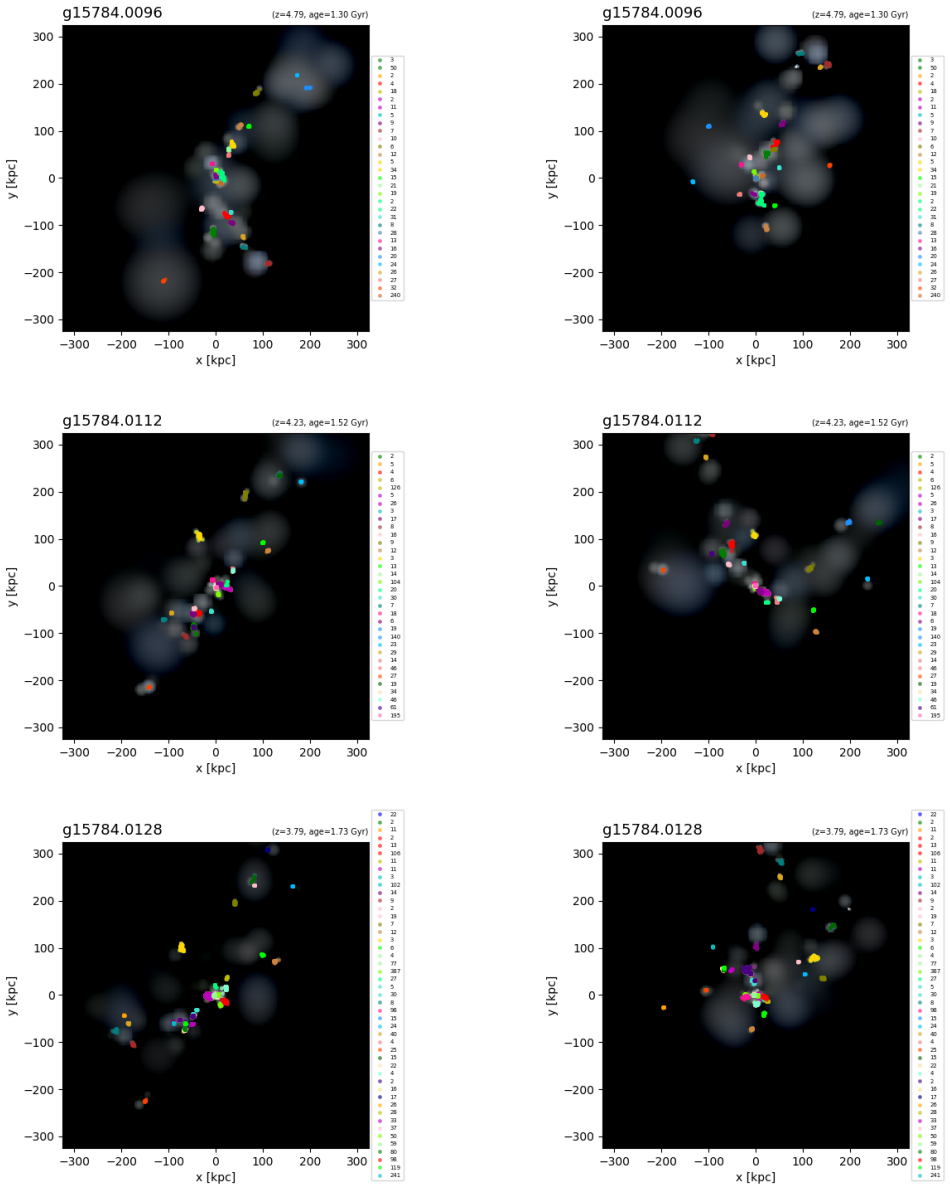

Figure 3.7: Satellite galaxies traced from higher redshift (above) to lower redshift (below). The redshifts range from z = 4.79 to z = 3.79. The first column (left) corresponds to a faced on perpective of the system and the second one (right) corresponds to an edge on perspective. All halos are shown with their current identification number in the snapshot at issue. The colour of each halo is the same than the original halo at high redshift thus, they can be distiguised by their colour. Here, new halos that have grown until having enough particles are taken into account to the tracing process.

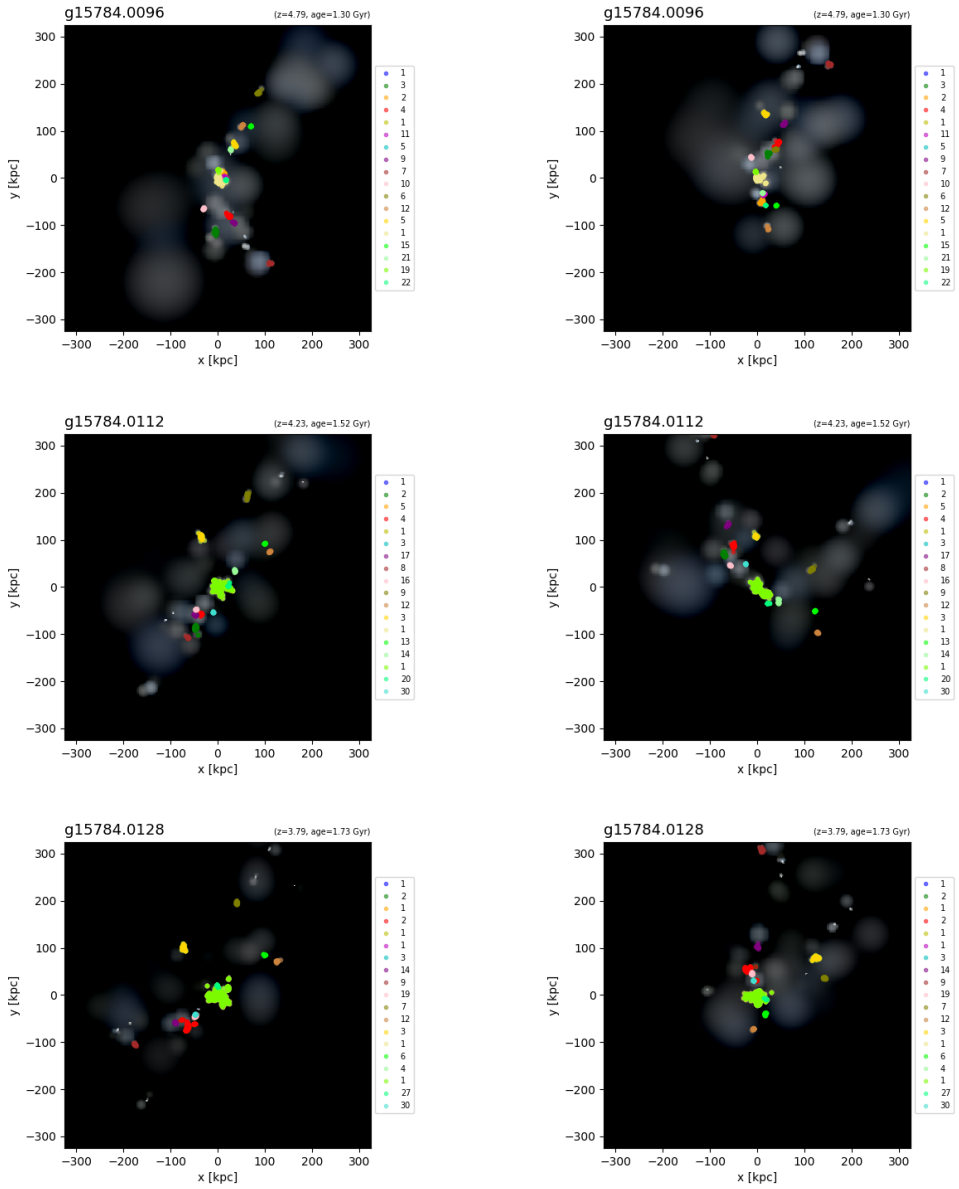

Figure 3.9: Satellite galaxies traced from higher redshift (above) to lower redshift (below) using the bridge method. The redshifts range from z = 4.79 to z = 3.79. The first column (left) corresponds to a faced on perpective of the system and the second one (right) corresponds to an edge on perspective. All halos are shown with their current identification number in the snapshot at issue. The colour of each halo is the same than the original halo at high redshift thus, they can be distiguised by their colour.

Chapter 4

Results and Discussion

Tras haber rastreado varias galaxias satélite hasta su momento de acreción dentro de la galaxia espiral, se han escogido ocho de estas galaxias acretadas en cuatro momentos diferentes de la simulación. Luego, se han anotado los valores de sus masas (estelar, gaseosa y de materia oscura) y se han tomado todas sus estrellas justo antes de comenzar a formar parte de la galaxia principal. Así, se ha podido plasmar las diferentes distribuciones de cada grupo de estrellas en el momento actual del Universo y compararlas según correspondan a galaxias satélites con tiempo de acreción menor o mayor, así como según sus diferentes masas/tamaños.

The final result of tracing the mergers through the different snapshots all the way to their time of accretion and then to their final disposition, was obtaining a certain distribution for each stellar group inside the main halo depending on several features. Therefore, it has been possible to pin down the current positions of some stars that formed outside the main halo (ex-situ stars) and have been accreted by the galaxy during its formation and evolution over the years.

To capture these final distributions, I used a sample of 8 satellites that got accreted into the main galaxy at four different times. Therefore, it has also been possible to compare between the distributions of satellites that merged at early times with others that merged much later. On the other hand, I have also compared the masses of each merger just before their accretion. These chosen satellites belong to the "merger epoch" of the simulated galaxy, in which the number of mergers was very high and the main halo was continuously attracting other bodies and matter.

4.1 Mergers at their time of accretion

Once I found the moment when several old stars of reference begin to take part of the main halo, I tagged its host halo as a merger and recorded its identification number in the time step right before it is fully accreted, along with its stellar mass, gaseous mass, dark matter mass and total mass. These values are presented in table 4.1, in which the snapshots and redshifts of accretion of each galaxy are also specified in the first column.

The mergers specified in table 4.1 have been accreted between the following redshift intervals: z = 5.53 - 4.79 (1.09 - 1.30 Gyr), z = 2.87 - 2.65 (2.37 - 2.59 Gyr), z = 2.28 - 2.13 (3.02 - 3.23 Gyr), and z = 1.76 - 1.66 (3.87 - 4.09 Gyr). As we can see the largest body corresponds to halo 2 in the snapshot 0192, with a total mass of 56950.40×10^6 solar masses. In fact, this merger is the biggest one of all the satellite galaxies that have been traced and indeed it represents the last major merger of the simulated Milky Way-like galaxy. This merger is compounded by many other halos of different masses and sizes that have gathered together since the earliest time considered here, illustrating the hierarchical formation of these structures. Additionally, halo 20, that got accreted in the snapshot 0304, is the union of two halos found in the first snapshot of study (snapshot 0080), correspondent to the value of z = 5.53. These two original halos can be seen in figure 3.5, coloured in cyan and yellow, and tagged with the identification numbers of 8 and 14, respectively.

Snapshot	**Accret. nº**	**S. Mass**	**G. Mass**	**D. Mass**	**T. Mass**
0096	2	25.74	1877.07	10745.72	12648.50
(z=4.79)	17	1.60	284.03	1759.42	2045.04
	65	1.53	107.30	480.24	589.08
0192	2	355.12	11124.90	45470.39	56950.40
(z=2.65)	20	56.41	1082.63	243.44	1382.49
0240	4	99.60	3600.90	21122.95	24823.50
(z=2.13)	6	31.58	2246.71	12382.30	14660.60
0304	20	76.25	504.33	2119.05	2699.63
(z=1.66)					

Table 4.1: Data of eight mergers at four different accretion times. In the first column, it is presented the number of the snapshot and its redshift when the satellite has already being accreted. The second column exposes the halo number of each merger in the snapshot right before the accretion. The rest of the data corresponds to the stellar mass, gaseous mass, dark matter mass and total mass, respectively, of each merger in the time step before the accretion. All masses are in 10^6 $M_\odot$ units.

From the analysis of many other mergers, it was possible to observe that in the early stages of the galaxy formation, when the number of accretions was more frequent, the halos tended to be larger, having high values of their total mass. At later times, most mergers had the tendency to be smaller and to have less amount of particles, losing even all of their gaseous mass due to the gravitational accretion by the main halo. Furthermore, there have been several cases where a halo does not simply merge, but then reemerges in a subsequent step and later, merges again. This can be the side effect stemming from the "old-star method", in which the chosen star is not well gravitationally bound to the centre of the halo and moves from the main halo to another and so on. It can also be a consequence of the caveats in the `AHF` halo finder mentioned in chapter 3.

4.2 Final stellar distribution of the mergers

In the following figures, the stellar particles stemming from the eight mergers of analysis are highlighted in their current positions inside the simulated Milky Way-like galaxy, i.e. at redshift zero (at a time of a 13.51 Gyr-old Universe). The first picture, figure 4.1, shows in different hues of blue the three earliest mergers chosen, which are also some of the less massive ones as we can confirm from table 4.1. Most of these stars are placed in a spheroidal-shaped distribution and are gathered at the galactic centre, where the bulge is located.

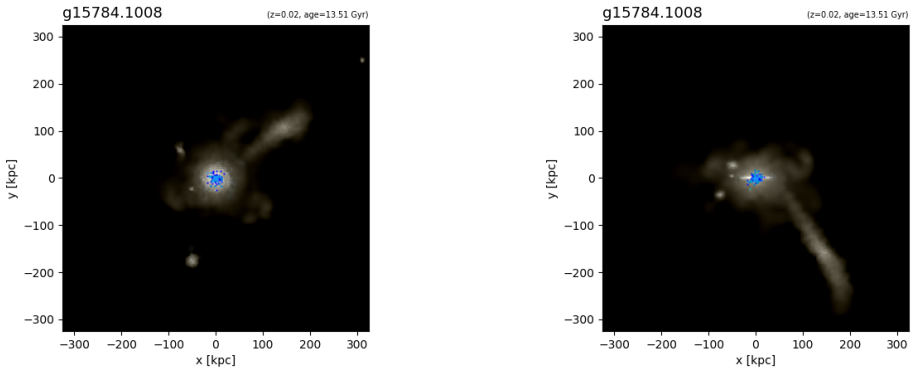

Figure 4.1: Stellar distribution of the three mergers in snapshot 0096 (between z = 5.53 and z = 4.79) at the current time in face on (left) and side on orientations (right). Halo 2 is coloured in blue, halo 17 in cyan, and halo 65 in dodger blue.

The next plot, figure 4.2, displays the following mergers of study. As for

the previous figure, both appear to form a spheroidal-like structure centered in the galactic nucleus. The yellow coloured stars belong to the largest merger mentioned in section 4.1, which seems to be rather spread throughout the main galaxy as the result of the big size of its progenitor satellite.

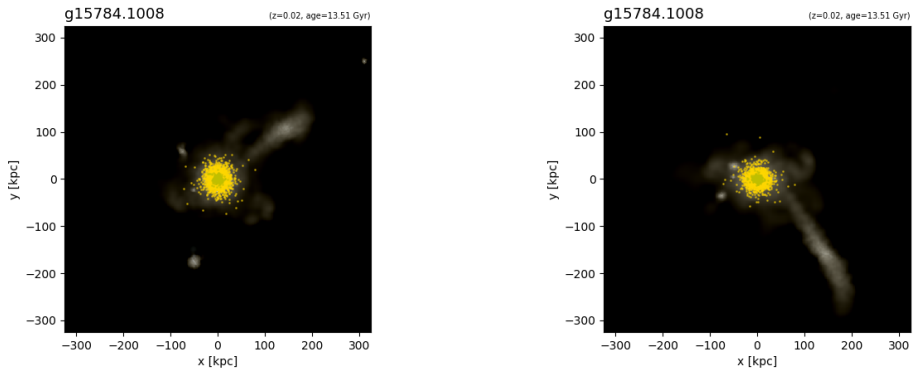

Figure 4.2: Stellar distribution of the mergers in snapshot 0192 (between z = 2.87 and z = 2.65) at the current time in face on (left) and side on orientations (right). Halo 2 is coloured in gold and halo 20 in dark yellow.

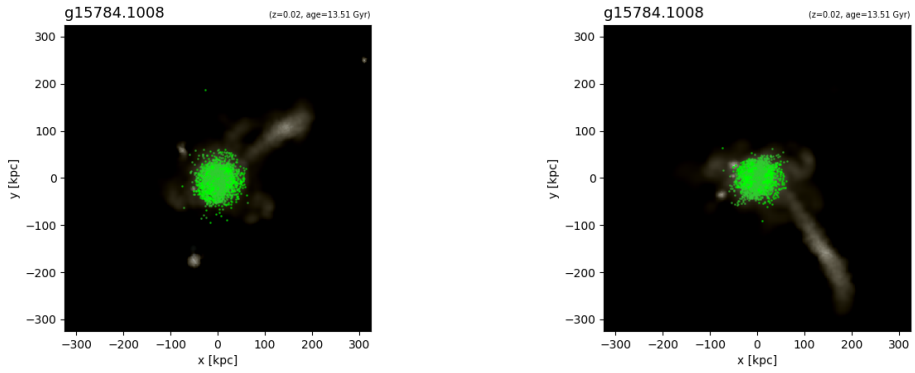

Figure 4.3: Stellar distribution of the mergers in snapshot 0240 (between z = 2.28 and z = 2.13) at the current time in face on (left) and side on orientations (right). Halo 4 is coloured in lime and halo 6 in green.

Thirdly, in figure 4.3, the two second most massive mergers, that got accreted in the snapshot 0240, are coloured in lime and green. It can be observed that the bigger one of both is highly scattered across the radial direction from the galactic centre. The other merger appears to be also

centered at the nucleus but shows an elongated structure almost parallel to the vertical direction, as we can observe in the side on orientation (right panel). This could be the result of a high angle (with respect to the disc) with which it was accreted.

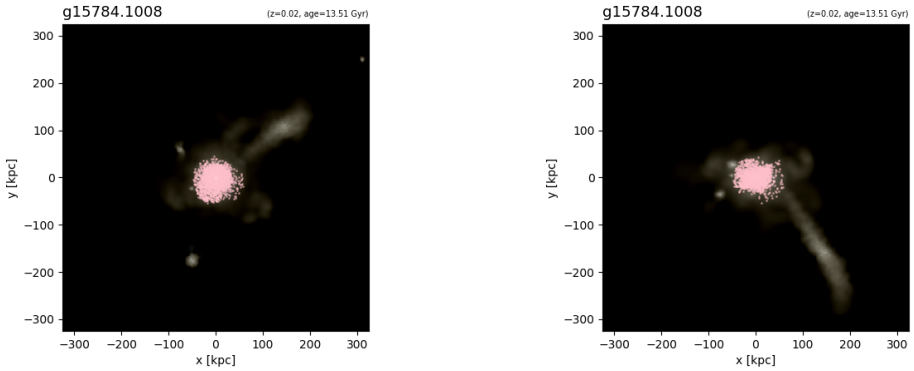

Figure 4.4: Stellar distribution of the merger in snapshot 0304 (between z = 1.76 and z = 1.66) at the current time in face on (left) and side on orientations (right), and coloured in pink .

Lastly, in figure 4.4, we can see the stellar distribution correspondent to the chosen merger that got accreted at lower redshift. This merger, which is amongst the less massive ones, is much more dispersed across the main halo than the other small mergers. It also seems to be slightly flattened in the edge on view with respect to the top view of the disc galaxy.

Other manner of visualising the different distributions of these mergers is to make a plot of their stellar density with respect to the radius of the main galaxy. This relation is shown in the graphic in figure 4.5[1] for the eight mergers of analysis, tagged with the same colours than for the previous figures. Then, we can see that for all of them the majority of the stars are concentrated at the centre of the galaxy and this amount of stellar particles decreases towards the outskirts, i.e. the stellar density is greater at lower values of the radius. Generally, the satellites that started becoming part of the main halo at later times are more spread out through the halo, although this seems to have some dependence on the mass of each merger at their time of accretion. If we compare the values exposed in table 4.1 with the results of the stellar density given in figure 4.5 we are able to see that the most massive halos present a less steep trend and cover more distance from the

[1]There is a misprint in the units of the vertical axis in figure 4.5. These are $[M_{\odot}/kpc^2]$.

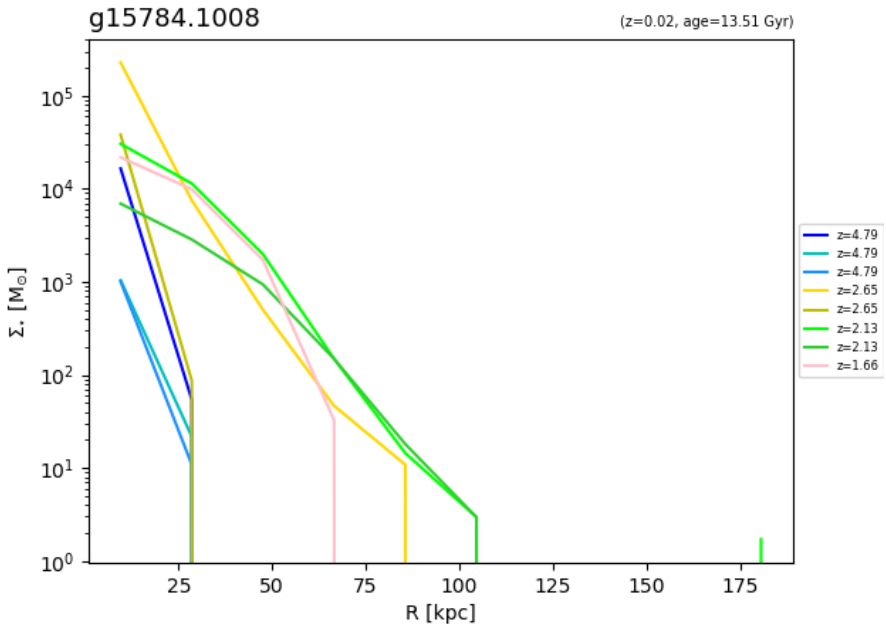

Figure 4.5: Density of stars from each merger with respect to the distance from the centre of the main galaxy. The vertical axis is scaled to logarithmic values, in units of solar masses per square kiloparsec. The different redshifts at which each merger got accreted are shown in the legend.

centre. On the contrary, the smaller mergers tend to be more collected near the centre. More detailed analysis would be to disentangle the effects of mass and accretion time, and account for the masses of the different components of each merger (stars, gas and dark matter) independently, as well as choosing more mergers with wider ranges for the redshifts and the masses.

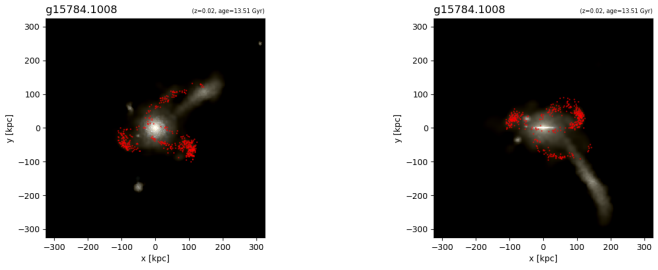

Figure 4.6: Stellar distribution of a late merger at the current time in face on (left) and side on orientations (right).

Regarding to the higher scattering in later mergers, it could be explained by the greater tidal forces and gravitational pull of the growing galaxy, that tends to tear apart and disperse the satellite at issue. This can also cause a total disruption of the merger resulting in tidal streams of stars that orbit the main halo. Additionally, later mergers have generally fallen from greater distances, meaning that they have higher gravitational potential energy at early times. One example of this is illustrated in figure 4.6, that shows an ongoing accretion of stars of a late merger that started to be accreted by the main galaxy at redshift of z = 0.82 (Universe of 6.87 Gyr). This merger is quite similar to the Sagittarius Dwarf Galaxy (Sgr) (Ibata, Gilmore, and Irwin, 1994) that is being swallowed by the Milky Way.

Chapter 5

Conclusion and Outlook

El procedimiento seguido en este trabajo ha permitido analizar la formación y evolución de una galaxia espiral simulada a partir de numerosas galaxias satélite para luego rastrear las estrellas originadas en ellas hasta sus posiciones finales. Además, se ha visto que estas distribuciones finales de estrellas dependen del tiempo de acreción y de la masa de cada galaxia progenitora. Estudios más detallados de los factores de los que dependen dichas distribuciones ayudarían a ver de forma más clara estas relaciones. Igualmente, la comparación de resultados obtenidos con simulaciones y resultados obtenidos a través de las observaciones proporcionan mucha información relevante sobre la formación de galaxias y sus pasados encuentros y colisiones.

Thanks to all the process developed in this project to track satellite galaxies and their stars (described in chapter 3) it has been possible to succesfully achieve the main goals stated for this work. Thus, this procedure, based on the concept of *Galactic Archaeology*, has allowed the analysis of the merger history of a simulated disc galaxy with similar mass to that of the Milky Way through the study of the chemical abundances of the stars, and through the visualisation of the evolution of the whole system from the early stages of its formation to its current state in the Universe nowadays in a cold dark matter cosmological environment. The results, given in chapter 4, allowed to establish the final positions of the stars originated in several satellite galaxies orbiting around the main one and situated within its virial radius, and also to compare these different distributions according to the time of accretion of each merger.

As it was mentioned in chapter 4, the final arrangement of the ex-situ

stars rely on the infall time of their progenitors into the main halo, but also on the mass of each one of these mergers. Although said relations can be seen clearly in these results, it would be interesting to visualise them through the analysis of a larger number of mergers with a wider variety of masses and accretion times. Therefore, it would be possible to make some graphics showing the masses of the different components of these mergers (stars, gas, dark matter and total mass) versus the final maximum radial positions of the stars, or even versus the mean density of stars per kiloparsec (or scattering) of each stellar group. Moreover, it would also be interesting to make a similar graphic with the redshift at which each merger is accreted instead of its mass to observe the distribution of the stars according to the moment when they started forming part of the main galaxy. However, as it has already being said, these distribution of stars also depend on many other elements like the angle of accretion, the velocity and orbits of the stars or their metallicities, so that it would also be appealing to do an analogous research for these magnitudes.

A more deeply series of analysis like the ones proposed above, would help us to study the origin of the different components of a typical disc galaxy (thin disc, thick disc, stellar halo, bulge, bar, etc.) and their composition in term of their stars (ages, metallicities, kinematics, etc), whether they come from the outer galaxy or they were formed in the proto-galaxy. This would also lead to more specific researches like the ones focused on unveiling the impact in the formation of galaxies from big mergers and collisions with other bodies, for instance, the ongoing merger of the Sagittarius Dwarf Galaxy in the Milky Way (Ibata et al., 1994), or its past encounter with the major merger known as Gaia-Encedalus (Chris B. Brook, Kawata, Gibson, and Flynn, 2003; Gallart et al., 2019; Helmi et al., 2018; etc.), as well as the structures found as a consequence of these massive events (e.g. Helmi, 2020). Comparing the results given in studies using cosmological simulations and the results with observations and data releases from multiple missions like *Gaia* (G. Collaboration et al., 2018), it is possible to keep on building an hypothetical scenario to understand the main processes of galaxy formation and evolution.

Bibliography

Brook, C. B. [C. B.], Stinson, G. S., Gibson, B. K., Kawata, D., House, E. L., Miranda, M. S., ... Quinn, T. R. (2012). Thin disc, thick disc and halo in a simulated galaxy. arXiv: 1206.0740 [astro-ph.GA]

Brook, C. B. [C. B.], Stinson, G. [G.], Gibson, B. K., Wadsley, J., & Quinn, T. (2012). Magicc disks: Matching observed galaxy relationships over a wide stellar mass range. arXiv: 1201.3359 [astro-ph.CO]

Brook, C. B. [Chris B.], Kawata, D., Gibson, B. K., & Flynn, C. (2003). Galactic halo stars in phase space: A hint of satellite accretion? *The Astrophysical Journal*, *585*(2), L125–L129. doi:10.1086/374306

Buck, T. (2018). On the formation of the milky way system in cosmological context - a numerical study. Retrieved from http://www.ub.uni-heidelberg.de/archiv/25607

Chabrier, G. (2003). Galactic Stellar and Substellar Initial Mass Function. *pasp*, *115*(809), 763–795. doi:10.1086/376392. arXiv: astro-ph/0304382 [astro-ph]

Collaboration, G., Brown, A. G. A., Vallenari, A., Prusti, T., de Bruijne, J. H. J., Babusiaux, C., & Bailer-Jones, C. A. L. (2018). Gaia data release 2. summary of the contents and survey properties. arXiv: 1804.09365 [astro-ph.GA]

Collaboration, P., Ade, P. A. R., Aghanim, N., Armitage-Caplan, C., Arnaud, M., Ashdown, M., ... Zonca, A. (2013). Planck 2013 results. xvi. cosmological parameters. arXiv: 1303.5076 [astro-ph.CO]

Ferland, G. J., Korista, K. T., Verner, D. A., Ferguson, J. W., Kingdon, J. B., & Verner, E. M. (1998). CLOUDY 90: Numerical Simulation of Plasmas and Their Spectra. *pasp*, *110*(749), 761–778. doi:10.1086/316190

Freeman, K., & Bland-Hawthorn, J. (2002). The new galaxy: Signatures of its formation. arXiv: astro-ph/0208106 [astro-ph]

Gallart, C., Bernard, E. J., Brook, C. B., Ruiz-Lara, T., Cassisi, S., Hill, V., & Monelli, M. (2019). The birth of the milky way as uncovered by accurate stellar ages with gaia. arXiv: 1901.02900 [astro-ph.GA]

Gill, S. P. D., Knebe, A., & Gibson, B. K. (2004). The evolution of substructure - I. A new identification method. *mnras*, *351*(2), 399–409. doi:10.1111/j.1365-2966.2004.07786.x. arXiv: astro-ph/0404258 [astro-ph]

Haardt, F., & Madau, P. (1996). Radiative Transfer in a Clumpy Universe. II. The Ultraviolet Extragalactic Background. *apj*, *461*, 20. doi:10.1086/177035. arXiv: astro-ph/9509093 [astro-ph]

Helmi, A. (2020). Streams, substructures and the early history of the milky way. arXiv: 2002.04340 [astro-ph.GA]

Helmi, A., Babusiaux, C., Koppelman, H. H., Massari, D., Veljanoski, J., & Brown, A. G. A. (2018). The merger that led to the formation of the milky way's inner stellar halo and thick disk. arXiv: 1806.06038 [astro-ph.GA]

Ibata, R. A., Gilmore, G., & Irwin, M. J. (1994). A dwarf satellite galaxy in Sagittarius. *nat*, *370*(6486), 194–196. doi:10.1038/370194a0

Kennicutt, J., Robert C. (1998). The Global Schmidt Law in Star-forming Galaxies. *apj*, *498*(2), 541–552. doi:10.1086/305588. arXiv: astro-ph/9712213 [astro-ph]

Knollmann, S. R., & Knebe, A. (2009). AHF: Amiga's Halo Finder. *apjs*, *182*(2), 608–624. doi:10.1088/0067-0049/182/2/608. arXiv: 0904.3662 [astro-ph.CO]

Majewski, S. R., Schiavon, R. P., Frinchaboy, P. M., Allende Prieto, C., Barkhouser, R., Bizyaev, D., ... Zamora, O. (2017). The Apache Point Observatory Galactic Evolution Experiment (APOGEE). *aj*, *154*(3), 94. doi:10.3847/1538-3881/aa784d. arXiv: 1509.05420 [astro-ph.IM]

Monaghan, J. J. (1992). Smoothed particle hydrodynamics. *Annual Review of Astronomy and Astrophysics*, *30*(1), 543–574. doi:10.1146/annurev.aa.30.090192.002551. eprint: https://doi.org/10.1146/annurev.aa.30.090192.002551

Penzias, A. A., & Wilson, R. W. (1965). A Measurement of Excess Antenna Temperature at 4080 Mc/s. *apj*, *142*, 419–421. doi:10.1086/148307

Pontzen, A., Roškar, R., Stinson, G. S., Woods, R., Reed, D. M., Coles, J., & Quinn, T. R. (2013). pynbody: Astrophysics Simulation Analysis for Python. Astrophysics Source Code Library, ascl:1305.002.

Robertson, B., & Kravtsov, A. (2007). Molecular hydrogen and global star formation relations in galaxies. arXiv: 0710.2102 [astro-ph]

Schmidt, M. (1959). The Rate of Star Formation. *apj*, *129*, 243. doi:10.1086/146614

Shen, S., Wadsley, J., & Stinson, G. (2009). The enrichment of the intergalactic medium with adiabatic feedback i: Metal cooling and metal diffusion. arXiv: 0910.5956 [astro-ph.CO]

Spergel, D. N., Bean, R., Doré, O., Nolta, M. R., Bennett, C. L., Dunkley, J., ... Wright, E. L. (2006). Wilkinson microwave anisotropy probe (wmap) three year results: Implications for cosmology. arXiv: astro-ph/0603449 [astro-ph]

Stinson, G. [G.], Bailin, J., Couchman, H., Wadsley, J., Shen, S., Brook, C., & Quinn, T. (2010). Cosmological galaxy formation simulations using sph. arXiv: 1004.0675 [astro-ph.CO]

Stinson, G. [G.], Brook, C., Macciò, A. V., Wadsley, J., Quinn, T. R., & Couchman, H. M. P. (2012). Making galaxies in a cosmological context: The need for early stellar feedback. arXiv: 1208.0002 [astro-ph.CO]

Stinson, G. [Greg], Seth, A., Katz, N., Wadsley, J., Governato, F., & Quinn, T. (2006). Star formation and feedback in smoothed particle hydrodynamic simulations – I. Isolated galaxies. *Monthly Notices of the Royal Astronomical Society*, *373*(3), 1074–1090. doi:10.1111/j.1365-2966.2006.11097.x. eprint: https://academic.oup.com/mnras/article-pdf/373/3/1074/18664536/mnras0373-1074.pdf

Wadsley, J. W., Stadel, J., & Quinn, T. (2004). Gasoline: a flexible, parallel implementation of TreeSPH. *na*, *9*(2), 137–158. doi:10.1016/j.newast.2003.08.004. arXiv: astro-ph/0303521 [astro-ph]

Wadsley, J. W., Veeravalli, G., & Couchman, H. M. P. (2008). On the treatment of entropy mixing in numerical cosmology. *Monthly Notices of the Royal Astronomical Society*, *387*(1), 427–438. doi:10.1111/j.1365-2966.2008.13260.x. eprint: https://academic.oup.com/mnras/article-pdf/387/1/427/3214920/mnras0387-0427.pdf